

SPG-VTON: Semantic Prediction Guidance for Multi-pose Virtual Try-on

Bingwen Hu, Ping Liu, *Member, IEEE*, Zhedong Zheng, and Mingwu Ren

Abstract—Image-based virtual try-on is challenging in fitting a target in-shop clothes into a reference person under diverse human poses. Previous works focus on preserving clothing details (*e.g.*, texture, logos, patterns) when transferring desired clothes onto a target person under a fixed pose. However, the performances of existing methods significantly dropped when extending existing methods to multi-pose virtual try-on. In this paper, we propose an end-to-end Semantic Prediction Guidance multi-pose Virtual Try-On Network (SPG-VTON), which could fit the desired clothing into a reference person under arbitrary poses. Concretely, SPG-VTON is composed of three sub-modules. First, a Semantic Prediction Module (SPM) generates the desired semantic map. The predicted semantic map provides more abundant guidance to locate the desired clothes region and produce a coarse try-on image. Second, a Clothes Warping Module (CWM) warps in-shop clothes to the desired shape according to the predicted semantic map and the desired pose. Specifically, we introduce a conductible cycle consistency loss to alleviate the misalignment in the clothes warping process. Third, a Try-on Synthesis Module (TSM) combines the coarse result and the warped clothes to generate the final virtual try-on image, preserving details of the desired clothes and under the desired pose. Besides, we introduce a face identity loss to refine the facial appearance and maintain the identity of the final virtual try-on result at the same time. We evaluate the proposed method on the most massive multi-pose dataset (MPV) and the DeepFashion dataset. The qualitative and quantitative experiments show that SPG-VTON is superior to the state-of-the-art methods and is robust to the data noise, including background and accessory changes, *i.e.*, hats and handbags, showing good scalability to the real-world scenario.

Index Terms—Virtual Try-on, Multi-pose, Semantic Prediction

I. INTRODUCTION

Image-based virtual try-on systems aim at fitting a target in-shop clothes into a reference person, which is a branch of the field of image synthesis. Driven by the rapid development of image synthesis [1]–[4], the topic of image-based virtual try-on has attracted more interest and has vast potential applications in virtual reality and human-computer interaction. Despite significant progress in the previous works [5]–[16] for virtual try-on, the multi-pose virtual try-on has not been well studied. Concretely, for a given person image, the virtual fitting system could generate realistic images of this person in different poses while preserving the desired clothes’ appearance. The multi-pose virtual fitting system is more in line with practical application scenarios. The existing works on multi-pose virtual fitting tasks are insufficient, and there are problems such as mismatch between the target clothes and the given pose, distortion of the clothes region in the try-on result, and loss of details that need to be further explored. To solve these

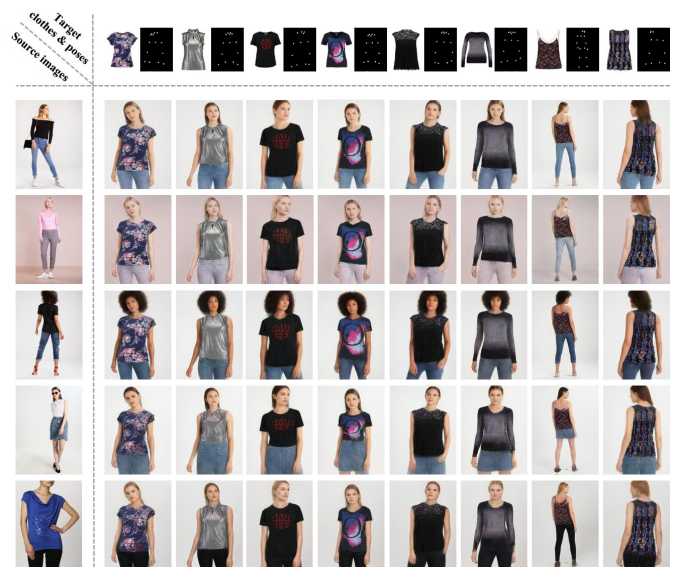


Fig. 1. Visual results of multi-pose virtual try-on by the proposed method. First column: the source images. Top row: in-shop clothes and target poses. Other columns: generated images. SPG-VTON produces photo-realistic virtual try-on results, which preserves both clothes details and person characteristics. Please zoom in to see the details of the generated images.

problems, we propose a method to build a robust multi-pose virtual try-on system based on 2D images (as shown in Fig. 1).

Most of the previous works [5], [6], [8], [9], [11], [12] focus on swapping clothes in a fixed pose without considering the body’s changing posture. However, in realistic scenarios, users would like to intuitively see the results of wearing the given clothes in different poses. Recently, MG-VTON [7] makes the first attempt at a virtual fitting system guided by multiple poses. MG-VTON is a multi-stage framework that includes a human parsing network, a warping generative adversarial network, and a refinement render network. Although MG-VTON takes a significant stride in virtual fitting system construction under arbitrary posture, it still has some limitations which restricts its further applications: (1) An end-to-end mechanism is missing in MG-VTON training process. In MG-VTON, modules designed with different purposes are utilized to generate the desired clothing deformation under different postures, a coarse result, and a refined result step by step. Each module/step is optimized independently and can not collaborate with others bidirectionally, which might cause a sub-optimal result; (2) In the inference process, MG-VTON requires multiple steps to generate the final results,

which might cost more human interventions and cause error accumulations. (3) MG-VTON only focuses on manipulation on body parts while ignoring the other parts, for example, faces. Missing a mechanism to process non-body parts makes their generated results not pleasant in nature and appearance.

To address the limitations mentioned above, we present a new multi-pose virtual try-on network which can work in an end-to-end manner. To make our method to handle variations introduced by arbitrary postures, we propose to introduce semantic prior knowledge into our network, making the learning process receive additional guidance from semantic prior knowledge. We name our designed method Semantic Prediction Guidance-Virtual Try On system, *a.k.a.*, SPG-VTON. As shown in Fig. 2, the SPG-VTON consists of three major modules, including the Semantic Prediction Module (SPM), the Clothes Warping Module (CWM), and the Try-on Synthesis Module (TSM). The purpose of the designed SPM is to predict the semantic map for target images, which is utilized to provide additional spatial and semantic guidance during the learning process. Given the semantic map for source images, the in-shop clothes, the target pose, and the predicted semantic map for the target image, a coarse result and corresponding predicted clothes mask are generated by SPM. CWM is introduced to warp the in-shop clothes to the desired shape according to the semantic map predicted by SPM. To alleviate the misalignment between the desired in-shop clothes and the target human posture, we propose to utilize a conductible cycle-consistency constraint in our network learning. Given the target pose, the coarse result generated by SPM, and the warped clothes generated by CWM, TSM generates the final try-on image in high precision and realism. Further, to make the generated results photo-realistic, we introduce a global discriminator and a local discriminator to control the global shape and local texture of generated results; to make the generated image visual pleasant, we utilize a face identity constraint to keep the synthesis face region realistic.

Extensive experiments on the MPV dataset [7] show that our method achieves superior performance to several existing approaches [5]–[7]. It is worth noting that what we studied in this work is currently the largest dataset for the multi-pose virtual try-on task. Since all images are collected from the Internet, the dataset inevitably contains much unexpected "label noise", such as misalignment and different backgrounds. The noise existing in web collected data inevitably compromises the training process in the dataset, making it challenging to train a robust virtual try-on system based on these noisy images. Benefiting from our designed method and exploration, we experimentally observe that the proposed method is still robust to such training noise, and demonstrates good scalability to the unseen test images during inference.

The main contributions of the proposed method are summarized as follows:

- We propose an end-to-end image-based multi-pose virtual try-on system called SPG-VTON, which could synthesis high-quality try-on images. Comparing to previous works, the proposed method could fit the desired clothing into a reference person under arbitrary poses while preserving details of the desired clothes.

- We conduct an extensive exploration and locate effective strategies for learning a robust and accurate virtual try-on network for multi-pose inputs. We introduce a conductible cyclic consistency loss to alleviate the misalignment in the clothes warping process. Concretely, the conductible cycle consistency loss could match the shape of the deformed desired clothes with the target person image and maintain characteristics of the desired clothes in the generated try-on image. In addition, we introduce both the global and local adversarial loss and the face identity loss to refine the facial appearance and maintain the identity of the final virtual try-on result at the same time. Moreover, we apply an end-to-end training strategy to boost the proposed method to generate accurate semantic maps and improve the virtual try-on results under pose transfer.
- The qualitative and quantitative experiments on two prevailing datasets, *i.e.*, MPV [7] and DeepFashion [17], demonstrate the advantages of our method in virtual try-on, especially when given different postures with heavy variations. The ablation studies also show the proposed method has good scalability to the unseen test data and robust to the label noise in the training set.

II. RELATED WORK

A. Pose-Guided Person Image Generation

Pose-guided person image generation is a practical yet challenging topic. In past years, Generative Adversarial Networks (GANs) [18] and various extensions [1]–[4], [19]–[23] make significant progresses in this research directions. However, due to the high variations existing in human poses and human appearance, these previous works [1]–[4], [19], [21], [22] are still suffering from their limited scalability in pose-guided person image generation. To generate high-quality person images in arbitrary poses, Ma *et al.* [24] proposes a two-stage generation framework. [24] first uses the U-Net-like network to produce initial images with blur, and then apply the adversarial way to refine coarse results. To further improve generated image qualities, Ma *et al.* proposes a *disentangling* strategy [25], encoding a given person image into three factors: pose, foreground, and background, respectively, which are decoded back to an image space after editing a specific factor. It is believed that manipulating those disentangled factors rather than treating them as a whole can benefit generation quality improvement. Zheng *et al.* disentangles the input pedestrian images into structure and appearance embedding, and can easily exchanges codes to generate source person with target clothes [26]. [27] also adopts the disentanglement strategy. In specific, they use a conditional U-Net architecture that combines the appearance decomposed from a variational autoencoder [28] with a given shape to reconstruct a new image. Methods such as [24], [25], [27] focus on the *global* pose deformation between the source image and the target image, while ignoring the *local* structure of generated images. Therefore these methods are hard to well maintain the local details of the original image, especially when there is a large pose discrepancy between the source image and the target

image. Recently, some works [9], [29]–[32] focus on the spatial deformation relationship in pose changes. [29] uses an inpainting network to estimate the coordinates in source images for elements of the body surface. Def-GAN [30] designs deformable skip connections in the generator to deal with the pixel-to-pixel misalignment caused by the pose differences. [9], [31], [32] employ a specific module to predict the human semantic map after the pose changed to align the source image with the target pose, which is to enforce module generates high-quality images. In this work, we also introduce a semantic map prediction model to produce the semantic map under a given pose. The difference is that when our method predicts the semantic map under a given pose, the clothing region of the semantic map changes with the given clothes. In contrast, the works mentioned above for pose-guided person image generation do not involve this aspect.

B. Virtual Try-on

The image-based virtual try-on task is a particular case of person generation. The core difference is that this task aims to generate a person image while the clothes region is changed to the desired clothes. The Thin-Plate Spline (TPS) [33] transformation is a typical 2-D interpolation model that performs geometric deformation between images by controlling a set of registration points between two images. VITON [5] directly applies the shape context-based matching [34] to estimate TPS transformation parameters between the mask of desired clothes and the clothes mask of the target person. Further, CP-VTON [6] uses a learnable method to estimate the TPS transformation parameters via convolutional neural networks dynamically. In the image-based virtual try-on task, using convolutional neural networks to learn the TPS transformation parameters between the desired clothes and the given human image is verified as a practical approach. The pioneering works [6]–[8], [10]–[12] mainly use two ways to estimate TPS transformation parameters. One way [6], [8], [10], is to use the geometric matching network [35] to estimate the TPS transformation parameters between the target clothing and the person representation (embedding the body shape, the target pose and reserved regions of the source image). Besides, these methods directly use the pixel-wise \mathcal{L}_1 -norm between the warped clothes and the clothes area extracted from the target image to train the geometric matching network. Another way [7], [11], [12] is to apply the geometric matching network to estimate the TPS transformation parameters between the clothes or clothes mask and the clothes area mask or the body shape obtained from the predicted semantic map. Similar to the first way, these methods also use the pixel-wise \mathcal{L}_1 -norm between the warped clothes and the clothes region extracted from the target person image to train the geometric matching network.

Although the methods mentioned above can produce high-quality fitting images to a certain extent, there is still a large gap between the generated images and natural images. For example, VITON [5] and CP-VTON [6] are state-of-the-art virtual try-on approaches that adopt a multi-stage coarse-to-fine strategy to tackle the virtual try-on task of the single

pose. However, neither of these two methods includes the change of human pose. In this case, these methods can not avoid the distortion and misalignment in the process of clothing deformation (such as the distortion and misalignment of texture, patterns, logos, and embroidery).

III. METHOD

We propose a novel image-based virtual try-on network named SPG-VTON, which focuses on multi-pose virtual try-on. Specifically, for a given source person image, a target in-shop clothes, and a target pose, the proposed method aims to generate a new person image that the same person wears the target in-shop clothes and preserves the target pose. That is, given different poses, the proposed method can generate high-quality virtual try-on images.

The SPG-VTON consists of three sub-modules, including the Semantic Prediction Module (Section III-B), the Clothes Warping Module (Section III-C), and the Try-on Synthesis Module (Section III-D). We show the overview of SPG-VTON in Fig. 2. Concretely, the SPM has two sequential processes. The first process of SPM aims to predict the semantic map of the target image according to the source semantic map, the in-shop clothes, and the target pose. The predicted semantic map provides precise guidance to locate the region of the desired clothes and generate a coarse virtual try-on image. Then, we combine the predicted semantic map, the in-shop clothes, and the target pose as the input of the second process of SPM to generate the coarse result and the predicted clothes mask. Subsequently, the CWM warps the in-shop clothes to the desired shape according to the predicted semantic map.

A. Person Representation

The diverse clothes and human poses struggle with the performance of the virtual try-on system. During the training process, the human pose and human body semantic map are critical supervision information for understanding the human geometric structure. For training images, we apply two off-the-shelf pose estimator [37] and human parser [38] to extract the human body keypoints and the semantic maps, respectively. The detailed process is as follows:

Human pose embedding. Following several off-the-shelf virtual try-on methods [5]–[9], [11], we use the pose estimator [37] to extract the pose of each person image. Then we obtain the coordinates of 18 human body keypoints from each person image and convert them to an 18 channel heatmap. Each channel of the heatmap corresponds to a human pose keypoint. We use each keypoint as the center of the circle to draw a circle with a radius of 4 pixels. The value in each circle is all ones, and the parts outside the circle are all zeros. In this way, we obtain the representation of the human pose embedding.

Human semantic map. Inspired by two semantic-guided virtual try-on approaches [7], [8], we extract human semantic maps of training images by using the existing human parser [38]. Each semantic map contains 20 labels that correspond to different parts of the human body. For intractable human body parts, such as the head (including the face

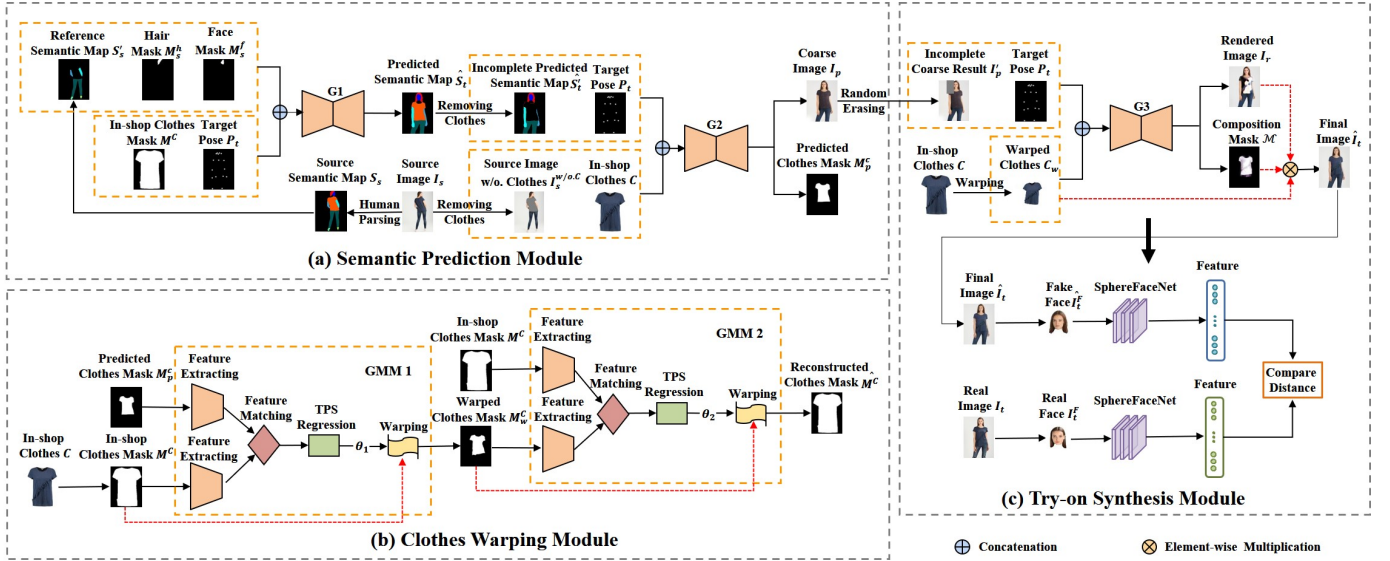


Fig. 2. The overview of our SPG-VTON. (a) The Semantic Prediction Model (SPM) consists of two processes. One is the target semantic map prediction, and the other one is the target clothes mask prediction and coarse result generation. (b) The Clothes Warping Module (CWM) warps the in-shop clothes to the shape of the clothes region of the target image, according to the Thin-Plate Spline (TPS) transformation parameters estimated between the mask of in-shop clothes and the predicted clothes mask. The CWM is composed of two Geometric Matching Modules (GMM) [35]. In specific, the GMM 1 deforms the mask of the in-shop clothes to the same shape with the predicted clothes mask, and then the GMM 2 is used to convert the warped clothes mask back to the mask of the desired clothes. Note that we do not directly apply the \mathcal{L}_1 -norm between the warped clothes mask and the predicted clothes, and \mathcal{L}_1 -norm between the reconstructed clothes and the original clothes mask to train GMM 1 and GMM 2. By contrary, we introduce a conductible cycle consistency loss to indirectly constrain GMM 1 and GMM 2, respectively (see III-C for details). (c) The Try-on Synthesis Module (TSM) combines the incomplete coarse results, the target pose, and the warped desired clothes to synthesis the final virtual try-on images. Also, the pre-trained SphereFaceNet [36] is applied to compare the distance between the generated face region and the ground-truth face region, which enforces the generator G_3 to generate realistic and natural faces.

and hair regions), it preserves characteristic personal identity information. The extracted information provided additional supervision signal for training our network.

B. Semantic Prediction Module

In order to precisely locate the clothes region of the generated person image and alleviate the mismatching between the target clothes and the generated human body, we introduce a Semantic Prediction Module (SPM). As shown in Fig. 2 a, SPM consists of two sequential processes and can be optimized in one step. The first process is the target semantic map prediction, the other is the target clothes mask and the coarse try-on result generation. First, given a source human image I_s and its corresponding semantic map S_s , a target in-shop clothes C , and a target human pose P_t , the first process of SPM is aims to predict the target human semantic map \hat{S}_t conditioned on the source semantic map S_s , the target clothes C , and the target pose P_t . Second, we combine the predicted semantic map \hat{S}_t with the desired clothes C , the target pose P_t , and the source image without clothes $I_s^{w/o.C}$, and then fed it into the second process of SPM to generate the coarse try-on image and the predicted clothes mask, respectively. Specifically, each process of the SPM is based on the conditional Generative Adversarial Network (cGAN) [19]. We adopt a ResNet-like network to replace the U-Net [39] structure as the generator G , and the multi-scale discriminator (PatchGAN) [3] is applied as the discriminator D . SPM contains two generators (i.e., G_1 and G_2) and two discriminators (i.e., D_1 and D_2). G_1 produces the predicted

semantic map of the target person that makes discriminator D_1 indistinguishable from the real image. Similarly, the role of generator G_2 is to generate the realistic coarse result and the predicted clothes mask. At the same time, discriminator D_2 attempts to distinguish real images from the results generated by G_2 . The network structure of generators and discriminators can be found in Table I.

Target semantic map prediction. We first define the head part as $A_s = \{M_s^f, M_s^h\}$, which composes of the face mask M_s^f and the hair mask M_s^h . A_s means that all the masks in A are obtained from the source semantic map S_s . Next, we remove the hair, face, and clothing areas from the source semantic map S_s to get the reference semantic map S'_s . Finally, we binarize the desired clothes image C to obtain the mask of desired clothes M^C . As shown in Fig. 2 (a), we combine the head part A_s with the reference semantic map S'_s , the mask of desired clothes M^C , and the target pose P_t as the input of the target semantic map prediction. Therefore, the predicted semantic map can be formulate as $\hat{S}_t = G_1(S'_s, A_s, M^C, P_t)$. To encourage the generated semantic map indistinguishable from the ground-truth semantic map, we introduce the spatial matching adversarial loss [18] as follows:

$$L_{adv}^s = \mathbb{E}[\log D_1(S_t, S'_s, A_s, M^C, P_t)] + \mathbb{E}[\log(1 - D_1(G_1(S'_s, A_s, M^C, P_t), S'_s, A_s, M^C, P_t))]. \quad (1)$$

In addition, to generate high-quality target semantic maps \hat{S}_t , we utilize the focal loss [38] on pixel-wise segmentation. Besides, following [7], [40], we also adopt the pixel-wise \mathcal{L}_1 -norm between the predicted semantic map and the target

semantic map to push the generator G_1 to produce smoother results. Therefore, the objective function to generate the target semantic map could be formulated as:

$$L_{seg} = L_{adv}^s + \lambda_1 L_{fl}^s + L_{recon}^s, \quad (2)$$

where L_{fl}^s denotes the focal loss between \hat{S}_t and S_t , L_{recon}^s denotes the pixel-wise \mathcal{L}_1 -norm between the predicted semantic map \hat{S}_t and the target semantic map S_t , and the hyper-parameter λ_1 control weights of the focal loss.

Target clothes mask prediction and coarse result generation. As shown in Fig. 2 (a), after obtaining the predicted semantic map \hat{S}_t from the first process of SPM, we first remove clothe region of \hat{S}_t to obtain the incomplete predicted semantic map \hat{S}'_t , and then combine \hat{S}'_t with the target pose P_t , the in-shop clothes C , and the source image without clothes $I_s^{w/o.C}$ as the input of the second process of SPM (*i.e.*, the input of the generator G_2). Then the generator G_2 produces both the coarse try-on image I_p and the predicted clothes mask M_p^c . To allow the generator to produce the photo-realistic coarse try-on image I_p , we also define the adversarial loss L_{adv}^p as follow:

$$L_{adv}^p = \mathbb{E}[\log D_2(I_t, \hat{S}_t, C, P_t, I_s^{w/o.C})] + \mathbb{E}[\log(1 - D_2(I_p, \hat{S}_t, C, P_t, I_s^{w/o.C}))]. \quad (3)$$

Following several start-of-the-art virtual try-on methods [5]–[9], [11], [12], we also adopt the perceptual loss [41] to enforce the generator G_2 to synthesize photo-realistic try-on images. The perceptual loss between I_p and I_t can be defined as:

$$L_{perc}^p = \mathbb{E}[\sum_{i=0}^5 \sigma_i \|\phi_i(I_p) - \phi_i(I_t)\|_1], \quad (4)$$

where $\phi_i(I)$ denotes the i -th layer feature map of the image I in the visual perception network ϕ . We apply the pre-trained VGG-19 [42] network as ϕ . Here five activations are utilized to calculate the perceptual loss. The hyper-parameters σ_i controls weights of the i -th layer to the term in Eq. 4. We apply the pixel-wise ℓ_1 loss to guide the target clothes mask prediction and the coarse result generation. Therefore, to minimize the distance between the generated image and the ground-truth image at the pixel level, we formulate the loss function as follow:

$$L_{recon}^p = \mathbb{E}[\|I_p - I_t\|_1] + \mathbb{E}[\|M_p^c - M_t^c\|_1], \quad (5)$$

where M_p^c represents the predicted clothes mask, and M_t^c denotes the clothes region mask exacted from the target human image I_t . The objective function to generate the coarse try-on result and target clothes mask could be formulated as:

$$L_{prd} = L_{adv}^p + \lambda_2(L_{recon}^p + L_{perc}^p), \quad (6)$$

where λ_2 control weights of L_{recon}^p and L_{perc}^p . Then the full objective function of the SPM can be defined as:

$$\begin{aligned} L_{spm} &= L_{seg} + L_{prd} \\ &= L_{adv}^s + \lambda_1 L_{fl}^s + L_{recon}^s \\ &\quad + L_{adv}^p + \lambda_2(L_{recon}^p + L_{perc}^p), \end{aligned} \quad (7)$$

C. Clothes Warping Module

The Clothes Warping Module (CWM) aims to fit the desired clothes into the target person according to the given pose while preserving the texture of clothes. Most existing works [6]–[8], [11] directly utilize a Geometric Matching Model (GMM) [35] to estimate the parameters of the Thin-Plate Spline (TPS) used to warp clothes. This strategy is applicable when the texture of the clothes is monotonous, and the target pose is fixed. However, when dealing with complex cases (*e.g.*, the desired clothes with complex texture and the target person under diversity poses), it might lead to misalignment between clothes and the human body, and blurred results. To address the challenges mentioned above, we introduce the conductible cycle consistency loss, which effectively aligns the desired clothing with a given pose.

As shown in Fig. 2 (b), we first apply the geometric matching network [35] to estimate the TPS transformation parameters θ_1 between the mask of desired clothes M^C and the predicted clothes mask M_p^c . The mask of desired clothes M^C is then warped using the transformation parameters θ_1 to align it with the predicted clothes mask M_p^c . We denote the operation of TPS transformation as \mathcal{T}_θ , and then the warped mask of desired clothes M_w^C can be represented as $M_w^C = \mathcal{T}_{\theta_1}(M^C)$. Next, the second geometric matching network is adopted to estimate the TPS transformation parameters θ_2 between the warped mask of desired clothes M_w^C and the mask of desired clothes M^C . We use the TPS transformation parameters θ_2 to warp M_w^C back to the original mask of desired clothes M^C . We denote the output of the second geometric matching network as $\hat{M}^C = \mathcal{T}_{\theta_2}(M_w^C)$.

Conductible cycle consistency loss. A straightforward solution is to train the geometric matching network by directly applying the pixel-level \mathcal{L}_1 -norm to encourage M_w^C approximates M_p^c and M^C approximates M^C to obtain the TPS transform parameters for the desired clothing deformation. However, using the self-reconstruction approach to estimate TPS parameters between the given clothes mask and the target clothes mask can only roughly align the shape of the given clothes mask with the target clothes mask. Applying the estimated parameters to warp the desired clothes directly can not preserve the details of the clothes well. Based on these observations, we introduce the conductible cycle consistency loss for two goals. One is to match the shape of the deformed desired clothes with the target person image. The other is to maintain the characteristics of the desired clothes in the clothing region of the generated try-on image. Specifically, we adopt the estimated parameters θ_1 to warp the desired clothes C to obtain the warped clothes $C_w = \mathcal{T}_{\theta_1}(C)$, and then use the estimated parameter θ_2 to warp C_w to produce $\hat{C} = \mathcal{T}_{\theta_2}(C_w)$. Thus, we formulate the conductible cycle consistency Loss as follow:

$$L_{cond} = \mathbb{E}[\|C_w - C_t\|_1] + \mathbb{E}[\|\hat{C} - C\|_1], \quad (8)$$

where C_t denotes the ground-truth clothes region exacted from the target image I_t . Then the full objective function of the CWM can be defined as:

$$L_{cwm} = \lambda_3 L_{cond}, \quad (9)$$

where λ_3 control weights of the conductible cycle consistency Loss.

Discussion. The existing methods [5]–[8], [11] adopt a separate clothing deformation module to calculate the TPS transformation parameters between the desired clothing and the target person image. The TPS transformation parameters are given by the pre-trained clothing deformation module, which cannot be dynamically adjusted for these parameters and lead to error stacking. Different from previous works [5]–[8], [11], we adopt an indirect approach to train the geometric matching network. Concretely, we first fed the mask of desired clothes and the predicted clothes mask of the target person image into the geometric matching network, then use the estimated TPS transformation parameters to warp the desired clothes. The pixel-wise \mathcal{L}_1 loss between the warped desired clothes and the ground-truth clothes extracted from the target person image as the constraint of the geometric matching network. Furthermore, we adopt the pixel-wise \mathcal{L}_1 -norm between \hat{C} and the desired clothes C to encourage the warped mask of desired clothes M_w^C can back to the original mask of desired clothes M^C . This indirect constraint strategy can achieve not only accurately geometric deformation between the desired clothes and the target person image under an arbitrary pose, but also preserve rich details of the clothing in the generated person image. The ablation study verifies the effectiveness of the conductible cycle consistency loss.

D. Try-on Synthesis Module

After producing the coarse try-on result I_p by SPM, we first randomly erasing a part of I_p to get the incomplete coarse result I'_p , and then we combine I'_p and the deformed desired clothes C_w obtained by CWM and the target pose P_t . Next, we directly fed them into the TSM to generate the final virtual try-on image \hat{I}_t . As shown in Fig. 2 (c), we use the generator G_3 to produce a rendered result I_r and a composition mask \mathcal{M} at the same time. The final virtual try-on result can be formulated as follow:

$$\hat{I}_t = C_w \odot \mathcal{M} + I_r \odot (1 - \mathcal{M}), \quad (10)$$

where $(I_r, \mathcal{M}) = G_3(I'_p, C_w, P_t)$. \odot represents the element-wise matrix multiplication, and the clothes part in the final try-on image can be denoted as $\hat{C}_t = C_w \odot \mathcal{M}$. The value of each element in \mathcal{M} is between 0 and 1. Following several start-of-the-art virtual try-on methods [6], [8], [11], [12], we apply both the self-reconstruction loss and the perceptual loss [41] to enforce the generated image \hat{I}_t approximates the target image I_t . We define the full reconstruction loss as:

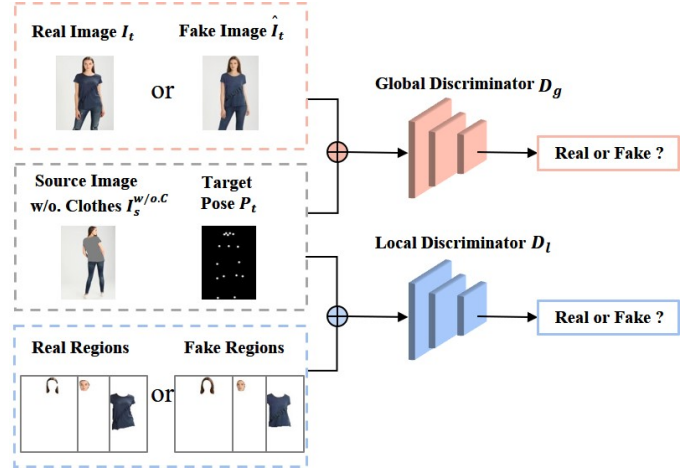


Fig. 3. The diagram of global and local discriminators. More details can be found at Table I.

$$L_{recon}^t = \alpha_1 \mathbb{E}[\|\hat{I}_t - I_t\|_1] + \alpha_2 \mathbb{E}[\|1 - \mathcal{M}\|_1], \quad (11)$$

where we adopt the second term in Eq. 11 as the regularization to constrain the generation of composition mask \mathcal{M} . We set $\alpha_1 = 2$, $\alpha_2 = 0.5$, respectively. Additionally, the perceptual loss between \hat{I}_t and I_t can be formulated as follow:

$$L_{perc}^t = \mathbb{E}[\sum_{i=0}^5 \sigma_i \|\phi_i(\hat{I}_t) - \phi_i(I_t)\|_1]. \quad (12)$$

Global and local adversarial loss. In the real scenario, it is difficult to obtain images of the same person wearing the desired clothes in arbitrary poses. Therefore, we cannot retain parts outside the clothes area follow many existing virtual try-on methods based on a fixed pose. In this case, to generate the photo-realistic try-on image, we employ a global adversarial loss and a local adversarial loss in TSM. The diagram of global and local discriminators is shown in Fig. 3. Specifically, we apply the global adversarial loss L_{adv}^g to enforce the generator G_3 to synthesis sharp virtual try-on images with global consistency. Furthermore, the local adversarial loss L_{adv}^l is adopted to refine the face area of the final result with local consistency. The global and local adversarial loss can be formulated as follow:

$$L_{adv}^g = \mathbb{E}[\log D_g(I_t, C_t, P_t, I_s^{w/o.C})] + \mathbb{E}[\log(1 - D_g(\hat{I}_t, \hat{C}_t, P_t, I_s^{w/o.C}))], \quad (13)$$

$$L_{adv}^l = \mathbb{E}[\log D_l(I_t^f, I_t^h, C_t, P_t, I_s^{w/o.C})] + \mathbb{E}[\log(1 - D_l(\hat{I}_t^f, \hat{I}_t^h, \hat{C}_t, P_t, I_s^{w/o.C}))], \quad (14)$$

where we extract the face region I_t^f and the hair region I_t^h from the ground-truth image I_t . In the same way, we also extract the face region \hat{I}_t^f , and the hair region \hat{I}_t^h from \hat{I}_t , respectively. D_g denotes the global discriminator, D_l denotes the local discriminator. D_g and D_l share the same structure.

Face identity loss. After adopting the global and local adversarial loss, our method can produce high-quality fitting

images while making the face region look natural. Furthermore, to enforce the face region cropped from the generated images similar to the face region of the related ground-truth images, we introduce the face identity loss.

$$L_{id} = \mathbb{E}[\|\mathcal{F}(\hat{I}_t^F) - \mathcal{F}(I_t^F)\|_1], \quad (15)$$

where \mathcal{F} denotes the pre-trained SphereFaceNet [36]. \hat{I}_t^F represents the face region extraction guided by the predicted semantic map, including the face part and the hair part. Then we formulate the full objective function of the TSM as:

$$L_{tsm} = \lambda_4(L_{recon}^t + L_{perc}^t) + L_{adv}^g + L_{adv}^l + \lambda_5 L_{id}, \quad (16)$$

where the hyper-parameter λ_4 controls weights of the reconstruction loss L_{recon}^t and the perceptual loss $L_{perc}(\hat{I}_t, I_t)$, and λ_5 control weights of the face identity loss L_{id} .

E. Optimization

Objective function. Taking all above loss functions into consideration, we formulate the total objective function as follow:

$$L_{total} = \underbrace{L_{adv}^s + \lambda_1 L_{fl}^s + L_{recon}^s + L_{adv}^p + \lambda_2 (L_{recon}^p + L_{perc}^p)}_{\text{SPM}} + \underbrace{\lambda_3 L_{cond}}_{\text{CWM}} + \underbrace{\lambda_4 (L_{recon}^t + L_{perc}^t) + L_{adv}^g + L_{adv}^l + \lambda_5 L_{id}}_{\text{TSM}}, \quad (17)$$

Our ultimate goal is to solve:

$$G^*, \mathcal{T}^* = \arg \min_{G_1, G_2, \mathcal{T}_{\theta_1}, \mathcal{T}_{\theta_2}, G_3} \max_{D_1, D_2, D_g, D_l} L_{total}, \quad (18)$$

End-to-end training. In this article, we divide the training process of the proposed method into three steps: (1) We first separately train the semantic prediction network to obtain the preliminary semantic prediction map, and this process corresponds to the first process of the semantic prediction module. (2) Then, we use the semantic prediction map generated from the fixed pre-trained semantic prediction network as guidance for the subsequent steps, including the rough results generation, the clothing area prediction, the target clothing deformation, and the refined try-on generation. (3) Finally, we jointly train three sub-modules of the proposed method to synthesize the final virtual try-on image. This step can alleviate the impact of inaccurate semantic maps and improve the quality of the generated results.

Differences from MG-VTON [7]. There are significant differences between MG-VTON. (1) MG-VTON adopts a multi-stage framework, and each stage independently implements a distinct task. In particular, MG-VTON applies different modules to achieve the desired clothing deformation, the coarse result generation, and the final result refinement separately. Instead, we employ end-to-end training to encourage the generator to produce realistic virtual try-on results. Specifically, we dynamically update the parameters of each process including the desired clothing deformation, the coarse result

generation, and the final result refinement. (2) MG-VTON divides the coarse result generation and the composition mask production into two independent steps. Different from it, we concatenate the coarse result, the warped clothes, and the target pose as the input of G_3 to produce a rendered result and a composition mask at the same time. And then, we combine the warped clothes, the rendered result, and the composition mask to synthesis the final result. Those differences make our method generate images with improved qualities in both qualitative and quantitative evaluations, which is demonstrated in Fig. 5, TABLE II and TABLE III.

IV. EXPERIMENTS

A. Dataset

We perform experiments on the MPV dataset [7], which is the largest multi-pose virtual fitting dataset available. The MPV dataset consists of 35,687 person images and 13,524 clothes images collected from Internet, with a resolution of 256×192 . For each in-shop clothes, the dataset contains multiple images of the same person wearing the given in-shop clothes in different poses. Moreover, we also conduct experiments on the DeepFashion dataset (*In-shop Clothes Retrieval Benchmark*) [17] to verify the effectiveness of the proposed method. Following the setting in MG-VTON [7], we collect 10,000 pairs (the same person in different poses) from DeepFashion, and random select in-shop clothes from the test set of the MPV dataset.

Noise in the training set and the test set. As shown in Fig. 4, we find three typical kinds of noise in both the training set and the test set, including interference of unrelated appearance attributes (*e.g.*, hats, bags, glasses), mismatching of clothes in paired person images with the same identity, and mismatching between the target clothes and the clothes in the source image. It is challenging to train a robust virtual fitting system based on these noisy images.

B. Evaluation Metrics

Structural SIMilarity (SSIM). SSIM [43] is widely used to evaluate the similarity of generated images in GAN-based methods. In this work, we adopt the SSIM metric to measure the similarity between the generated image and the real image. Higher scores indicate that the generated image is closer to the ground-truth image.

Inception Score (IS). IS [44] is a general metric be used to estimate the quality of the synthesis image. In this work, we apply IS to evaluate the quality of generated images by our method. Notably, all generated images are used to calculate IS have no corresponding ground-truth images.

To evaluate the quality of specific regions (*i.e.*, clothing regions, face regions) in the final virtual try-on image, we also calculate the Mask-SSIM and the Mask-IS for the extracted regions.

C. Implementation Details

Architecture. Here we provide details about the network architecture of three sub-modules in SPG-VTON. In specific,

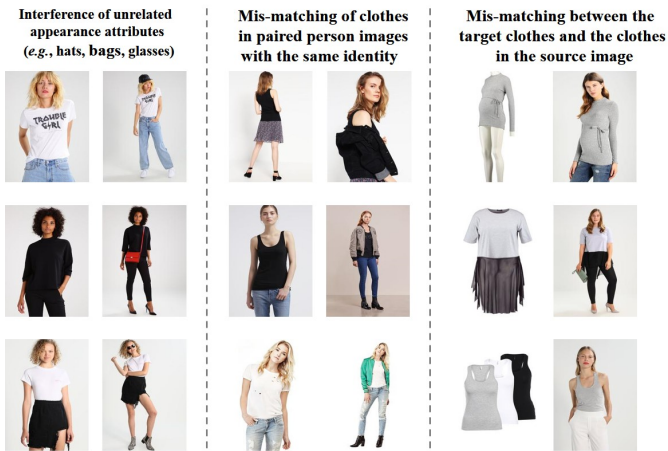


Fig. 4. Examples of noisy images in the training set and the test set. We observe the three typical kinds of noise existing in the training set and the test set, including interference of unrelated appearance attributes (e.g., hats, bags, glasses), mismatching of clothes in paired person images with the same identity, and mismatching between the target clothes and the clothes in the source image. These noise demands strong robust ability of the proposed algorithm during both training and testing.

generators G_1 , G_2 , and G_3 adopt the same structure, which is a ResNet-like architecture. The generated result of G_2 and G_3 is a 4-channel tensor that could be split into a 1-channel mask and a 3-channel RGB image. We show the detailed network structure of generators and discriminators in TABLE I. Besides, all the discriminators in the proposed method apply the multi-scale structure from pix2pixHD [3]. Additionally, we use instance normalization [45] both in generators and discriminators. We employ ReLU and LeakyReLU activation functions in the generator and discriminator, respectively. Following existing works [26], [46], we adopt LSGAN [47] for all adversarial losses in our method, and a gradient punishment strategy [48] is also used to stabilize the training process.

Setting. In this work, we use Adam optimizer [49] to optimize generators and discriminators in SPG-VTON, and set the initial learning rate to 0.0002, weight decay to 0.0005, and exponential decay rates $(\beta_1, \beta_2) = (0, 0.999)$. For training, we set hyper-parameters $\lambda_i = 10$, ($i = 1, 2, 4, 5$), and $\lambda_3 = 20$. Additionally, we set the batch size of semantic map prediction (first process of SPM, generator G_1) to 16, and the batch size of subsequent steps (generators G_2 and G_3 , geometric matching models GMM 1 and GMM 2) to 8, and the batch size for joint training is set to 8. In end-to-end training, we train the semantic map prediction network for $70k$, and then with the fixed pre-trained semantic map prediction network, the subsequent network is trained for $70k$. Finally, we jointly train the whole model for $100k$.

D. Quantitative Results

We compare the proposed method with several start-of-the-art virtual try-on methods, including VITON [5], CP-VTON [6], and MG-VTON [7]. VITON and CP-VTON adopt a coarse-to-fine strategy to tackle the virtual try-on task of the single pose, and neither of these two methods includes the change of human pose. To make a fair comparison, we

TABLE I
THE NETWORK ARCHITECTURE OF OUR GENERATORS AND DISCRIMINATORS, WHERE K, S, P, AND A DENOTE THE KERNEL SIZE, STRIDE SIZE, PADDING SIZE, AND THE ACTIVATION FUNCTION, RESPECTIVELY. **IN** REPRESENTS THE INPUT CHANNELS, AND **OUT** DENOTES THE OUTPUT CHANNELS. THE GENERATORS G_1 , G_2 , G_3 ADOPT THE SAME STRUCTURE WHILE THE INPUT CHANNELS AND OUTPUT CHANNELS ARE DIFFERENT. BESIDES, DISCRIMINATORS D_1 , D_2 , D_g , D_l SHARE THE SAME STRUCTURE WHILE THE INPUT CHANNELS ARE DIFFERENT.

Generator G_i			
Layer	Input	Output	K & S & P & A
Conv1	IN $\times 256 \times 192$	$64 \times 256 \times 192$	$3 \times 3, 1, 1, \text{ReLU}$
Conv2	$64 \times 256 \times 192$	$128 \times 256 \times 192$	$3 \times 3, 1, 1, \text{ReLU}$
Conv3	$128 \times 256 \times 192$	$128 \times 128 \times 96$	$3 \times 3, 2, 1, \text{ReLU}$
Resblock	$128 \times 128 \times 96$	$128 \times 128 \times 96$	$3 \times 3, 3 \times 3, 1, 1, \text{ReLU}$
Conv4	$128 \times 128 \times 96$	$256 \times 64 \times 48$	$3 \times 3, 2, 1, \text{ReLU}$
Resblock	$256 \times 64 \times 48$	$256 \times 64 \times 48$	$3 \times 3, 3 \times 3, 1, 1, \text{ReLU}$
Conv5	$256 \times 64 \times 48$	$512 \times 32 \times 24$	$3 \times 3, 2, 1, \text{ReLU}$
Resblock $\times 4$	$512 \times 32 \times 24$	$512 \times 32 \times 24$	$3 \times 3, 3 \times 3, 1, 1, \text{ReLU}$
Upsample	$512 \times 32 \times 24$	$512 \times 64 \times 48$	-
Conv6	$512 \times 64 \times 48$	$256 \times 64 \times 48$	$3 \times 3, 1, 1, \text{ReLU}$
Upsample	$256 \times 64 \times 48$	$256 \times 128 \times 92$	-
Conv7	$256 \times 128 \times 92$	$128 \times 128 \times 92$	$3 \times 3, 1, 1, \text{ReLU}$
Upsample	$128 \times 128 \times 92$	$128 \times 256 \times 192$	-
Conv8	$128 \times 256 \times 192$	$64 \times 256 \times 192$	$3 \times 3, 1, 1, \text{ReLU}$
Conv9	$64 \times 256 \times 192$	OUT $\times 256 \times 192$	$3 \times 3, 1, 1, \text{ReLU}$
Conv10	OUT $\times 256 \times 192$	OUT $\times 256 \times 192$	$3 \times 3, 1, 1, \text{Tanh}$
Conv11	OUT $\times 256 \times 192$	OUT $\times 256 \times 192$	$1 \times 1, 1, 0, \text{None}$
Discriminator D_i			
Layer	Input	Output	K & S & P & A
Conv1	IN $\times 256 \times 192$	$32 \times 256 \times 192$	$3 \times 1, 1, 0, \text{LeakyReLU}$
Conv2	$32 \times 256 \times 192$	$32 \times 256 \times 192$	$3 \times 3, 1, 1, \text{LeakyReLU}$
Conv3	$32 \times 256 \times 192$	$32 \times 128 \times 96$	$3 \times 3, 2, 1, \text{LeakyReLU}$
Conv4	$32 \times 128 \times 96$	$32 \times 128 \times 96$	$3 \times 3, 2, 1, \text{LeakyReLU}$
Conv5	$32 \times 128 \times 96$	$64 \times 64 \times 48$	$3 \times 3, 2, 1, \text{LeakyReLU}$
Conv6	$64 \times 64 \times 48$	$1 \times 64 \times 48$	$1 \times 1, 1, 0, \text{None}$

TABLE II
QUANTITATIVE RESULTS. COMPARISON RESULTS IN TERMS OF SSIM AND IS ON BOTH MPV AND DEEPPASHION. \uparrow DENOTES THAT HIGHER SCORES ARE BETTER.

Method	MPV		DeepFashion
	SSIM \uparrow	IS \uparrow	IS \uparrow
Real data	1.000	3.391 ± 0.024	3.332 ± 0.126
VITON [5]	0.639	2.394 ± 0.205	2.302 ± 0.116
CP-VTON [6]	0.705	2.519 ± 0.107	2.459 ± 0.212
MG-VTON [7]	0.744	3.154 ± 0.142	3.030 ± 0.057
SPG-VTON (Ours)	0.752	3.243 ± 0.127	3.124 ± 0.027

first enrich the input of VITON and CP-VTON by adding the target pose. We report the quantitative results based on the SSIM and IS metrics (higher scores are better) to evaluate the realism of the synthesized virtual try-on images. As shown in TABLE II, our method achieves the maximum SSIM scores and the maximum IS score on the MPV dataset. Besides, our method also obtains the highest IS scores on the DeepFashion dataset. The results verify the effectiveness of the proposed method on generating high-fidelity virtual try-on images.

Comparison with MG-VTON [7]. The multi-pose virtual try-on task aims to fit the desired clothes into the target person image, according to the source image, and the given pose. Unlike the pose fixed virtual try-on issue, the multi-



Fig. 5. Visualized comparison between MG-VTON [7] and several variants of our method on the MPV dataset. To make the comparison clearer, we use the green dashed box and the yellow dashed box to cut out the local areas of generated images by MG-VTON and SPG-VTON, respectively. And then enlarge them to 3.5 times the original size.



Fig. 6. Qualitative visual results with/without the cycle consistency constraint.

TABLE III

SPG-VTON v.s. MG-VTON [7]. QUANTITATIVE COMPARISON RESULTS IN TERMS OF MASK-SSIM AND MASK-IS ON THE PART OF MPV. \uparrow DENOTES THAT HIGHER SCORES ARE BETTER. NOTABLY, THE SOURCE IMAGE AND TARGET POSE IN EACH TUPLE IN THE TEST SET HAVE THE SAME IDENTITY, SO WE CALCULATE THE MASK-SSIM VALUES OF THE FACIAL AREA AND THE AREA UNRELATED TO CLOTHES BETWEEN THE GENERATED IMAGE AND THE ORIGINAL POSE IMAGE THAT PROVIDES THE TARGET POSE.

Method	Mask-SSIM \uparrow		Mask-IS \uparrow	
	Face	w/o Clothes	Face	Clothes
Real data	1.000	1.000	1.848 ± 0.137	3.711 ± 0.237
MG-VTON [7]	0.717 ± 0.094	0.722 ± 0.045	1.419 ± 0.061	3.270 ± 0.409
SPG-VTON (Ours)	0.737 ± 0.091	0.745 ± 0.042	1.584 ± 0.053	3.660 ± 0.327

pose virtual try-on task is much challenging to synthesis the whole try-on image, which does not preserve the original body parts. Since the existing methods (such as VITON [5] and CP-VTON [6]) based on the fixed pose that could not find the spatial deformation relationship in pose changed, therefore, directly applying these methods are inappropriate. MG-VTON is the first method to deal with the multi-pose virtual fitting issue. Hence, to further verify the effectiveness of this method, we conduct additional experiments to compare our method with MG-VTON on the MPV dataset. Consequently, we evaluate both the global metrics SSIM and IS, and the local indicators Mask-SSIM and Mask-IS, which estimate the local (*i.e.*, face

region and clothes region) similarity and local realism between the generated image and the ground-truth image. Without the official code of MG-VTON, we calculate the results of MG-VTON from the try-on images provided by the original author. Note that these try-on images are generated from part of the test set. To make a fair comparison, we obtain our results from the same test images. Each test sample consists of three-tuples, including the source images, the target poses, and the desired clothes. The source image and target pose in each tuple in the test set have the same identity, so we calculate the Mask-SSIM value between the generated image and the image corresponding to the target pose. Specifically, we calculate the Mask-SSIM of the facial area and the area unrelated to clothes between the generated image and the original image that provides the target pose. As shown in TABLE III, the proposed method achieves the higher Mask-SSIM scores and Mask-IS scores than MG-VTON, suggesting that our method is better at fitting the desired clothes into the target human image.

E. Qualitative Results

We present the visualized comparison between MG-VTON and several variants of our method on the MPV dataset in Fig. 5. We observe that our method achieves high-quality try-on results than MG-VTON. In particular, our method could

TABLE IV
 QUANTITATIVE RESULTS OF DIFFERENT VARIANTS OF SPG-VTON ON THE MPV DATASET. WE HIGHLIGHT THE **BEST** AND THE **SECOND-BEST** PERFORMANCES. \uparrow DENOTES THAT HIGHER SCORES ARE BETTER. THE VARIANT OURS W/ S_t REPRESENTS THAT OUR METHOD USES THE GROUND-TRUTH SEMANTIC MAP S_t OF THE TEST IMAGES TO REPLACE THE PREDICTED SEMANTIC MAP \hat{S}_t .

Method	SSIM \uparrow	IS \uparrow	Mask-SSIM \uparrow		Mask-IS \uparrow	
			Face	Clothes	Face	Clothes
Real data	1.000	3.391 \pm 0.024	1.000	1.000	2.255 \pm 0.030	5.094 \pm 0.084
Ours (<i>full</i>)	0.752 \pm 0.084	3.243 \pm 0.127	0.801 \pm 0.127	0.877 \pm 0.076	1.982 \pm 0.024	5.057 \pm 0.064
w/o <i>E2E</i>	0.747 \pm 0.087	2.968 \pm 0.031	0.795 \pm 0.130	0.869 \pm 0.081	1.976 \pm 0.013	4.854 \pm 0.019
w/o <i>Cycle</i>	0.739 \pm 0.086	2.745 \pm 0.036	0.794 \pm 0.127	0.867 \pm 0.080	1.801 \pm 0.016	4.841 \pm 0.096
w/o \hat{S}_t	0.736 \pm 0.088	2.647 \pm 0.017	0.794 \pm 0.129	0.861 \pm 0.083	1.856 \pm 0.009	4.796 \pm 0.027
w/o L_{id}	0.732 \pm 0.085	2.909 \pm 0.069	0.780 \pm 0.135	0.866 \pm 0.080	1.969 \pm 0.045	4.601 \pm 0.070
w/o L_{adv}^l	0.700 \pm 0.079	3.358 \pm 0.022	0.786 \pm 0.132	0.866 \pm 0.080	1.830 \pm 0.017	4.546 \pm 0.047
w/o L_{perc}	0.724 \pm 0.086	3.474 \pm 0.052	0.798 \pm 0.129	0.866 \pm 0.081	2.056 \pm 0.015	5.373 \pm 0.077
w/ S_t	0.788 \pm 0.080	3.165 \pm 0.028	0.893 \pm 0.081	0.923 \pm 0.063	2.070 \pm 0.013	5.186 \pm 0.071

TABLE V
 QUANTITATIVE RESULTS OF THE EFFECTIVENESS OF FIVE HYPER-PARAMETERS. WE HIGHLIGHT THE **BEST** PERFORMANCES. \uparrow DENOTES THAT HIGHER SCORES ARE BETTER.

λ	SSIM \uparrow	IS \uparrow	Mask-SSIM \uparrow		Mask-IS \uparrow	
			Face	Clothes	Face	Clothes
$\lambda_1 = 0$	0.714 \pm 0.078	2.983 \pm 0.042	0.781 \pm 0.131	0.852 \pm 0.086	1.796 \pm 0.006	4.916 \pm 0.090
$\lambda_2 = 0$	0.554 \pm 0.105	3.985 \pm 0.052	0.784 \pm 0.136	0.859 \pm 0.081	2.121 \pm 0.032	4.771 \pm 0.048
$\lambda_3 = 0$	0.739 \pm 0.085	2.581 \pm 0.016	0.792 \pm 0.130	0.869 \pm 0.078	1.836 \pm 0.018	4.151 \pm 0.024
$\lambda_4 = 0$	0.420 \pm 0.015	3.526 \pm 0.059	0.775 \pm 0.136	0.857 \pm 0.083	2.028 \pm 0.013	4.858 \pm 0.042
$\lambda_5 = 0$	0.732 \pm 0.085	2.909 \pm 0.069	0.780 \pm 0.135	0.866 \pm 0.080	1.969 \pm 0.045	4.601 \pm 0.070
Ours (<i>full</i>)	0.752 \pm 0.084	3.243 \pm 0.127	0.801 \pm 0.127	0.877 \pm 0.076	1.982 \pm 0.024	5.057 \pm 0.064

TABLE VI
 QUANTITATIVE RESULTS. WE HIGHLIGHT THE **BEST** PERFORMANCES. \uparrow DENOTES THAT HIGHER SCORES ARE BETTER.

λ_3	SSIM \uparrow	IS \uparrow	Mask-SSIM \uparrow		Mask-IS \uparrow	
			Face	Clothes	Face	Clothes
$\lambda_3 = 0$	0.739 \pm 0.085	2.581 \pm 0.016	0.792 \pm 0.130	0.869 \pm 0.078	1.836 \pm 0.018	4.151 \pm 0.024
$\lambda_3 = 1$	0.747 \pm 0.087	2.865 \pm 0.017	0.795 \pm 0.131	0.869 \pm 0.081	1.905 \pm 0.019	4.869 \pm 0.069
$\lambda_3 = 5$	0.745 \pm 0.087	2.929 \pm 0.081	0.794 \pm 0.131	0.869 \pm 0.081	2.008 \pm 0.022	4.749 \pm 0.097
$\lambda_3 = 10$	0.744 \pm 0.086	2.959 \pm 0.033	0.793 \pm 0.129	0.868 \pm 0.082	2.003 \pm 0.020	4.849 \pm 0.097
$\lambda_3 = 20$	0.752 \pm 0.084	3.243 \pm 0.127	0.801 \pm 0.127	0.877 \pm 0.076	1.982 \pm 0.024	5.057 \pm 0.064
$\lambda_3 = 40$	0.746 \pm 0.087	2.918 \pm 0.026	0.795 \pm 0.140	0.868 \pm 0.081	1.963 \pm 0.017	4.809 \pm 0.087
$\lambda_3 = 80$	0.746 \pm 0.086	2.910 \pm 0.028	0.794 \pm 0.131	0.869 \pm 0.080	1.952 \pm 0.030	4.934 \pm 0.012

generate realistic and natural face regions while preserving the desired clothes’ details.

F. Ablation Studies

To study the effectiveness of each component in our method, we compare seven variants of SPG-VTON on the MPV dataset as follows: (1) w/o *E2E*: our method without End-to-End training. Specifically, we train our method in a two-stage manner. We first separately train the semantic prediction network to obtain the preliminary semantic prediction map. Next, we use the semantic prediction map generated from the fixed pre-trained semantic prediction network to guide the subsequent steps; (2) w/o *Cycle*: our method uses \mathcal{L}_1 loss between M_w^c and M_p^c to replace the conductible cycle consistency loss in the CWM. In this case, $L_{cond} = \mathbb{E}[\|C_w - C_t\|_1]$; (3) w/o \hat{S}_t : our method without the predicted semantic map \hat{S}_t . In the training process, we use the predicted target body

shape M_p^b to replace the predicted semantic map \hat{S}_t ; (4) w/o L_{id} : our method removes the face identity loss. In this case, $L_{tsm} = \lambda_4(L_{recon}^t + L_{perc}^t) + L_{adv}^g + L_{adv}^l$; (5) w/o L_{adv}^l : our method without the local adversarial loss. In this case, $L_{tsm} = \lambda_4(L_{recon}^t + L_{perc}^t) + L_{adv}^g + \lambda_5 L_{id}$; (6) w/o L_{perc} : our method without the perceptual loss L_{perc}^p and the perceptual loss L_{perc}^t . In this case, $L_{spm} = L_{adv}^s + \lambda_1 L_{fl}^s + L_{recon}^s + L_{adv}^p + \lambda_2 L_{recon}^p$, and $L_{tsm} = \lambda_4(L_{recon}^t) + L_{adv}^g + L_{adv}^l + \lambda_5 L_{id}$; (7) w/ S_t : our method uses the ground-truth semantic map S_t of the test images to replace the predicted semantic map \hat{S}_t .

We show the qualitative results of seven variants in Fig. 5. We observe that without end-to-end training, our method can still produce plausible results. However, some artifacts existed near the hair regions and the neck regions in generated images, suggesting that the end-to-end training manner could alleviate the impact of incorrect semantic maps on the generated results. We also find that without the cycle consistency constraint,

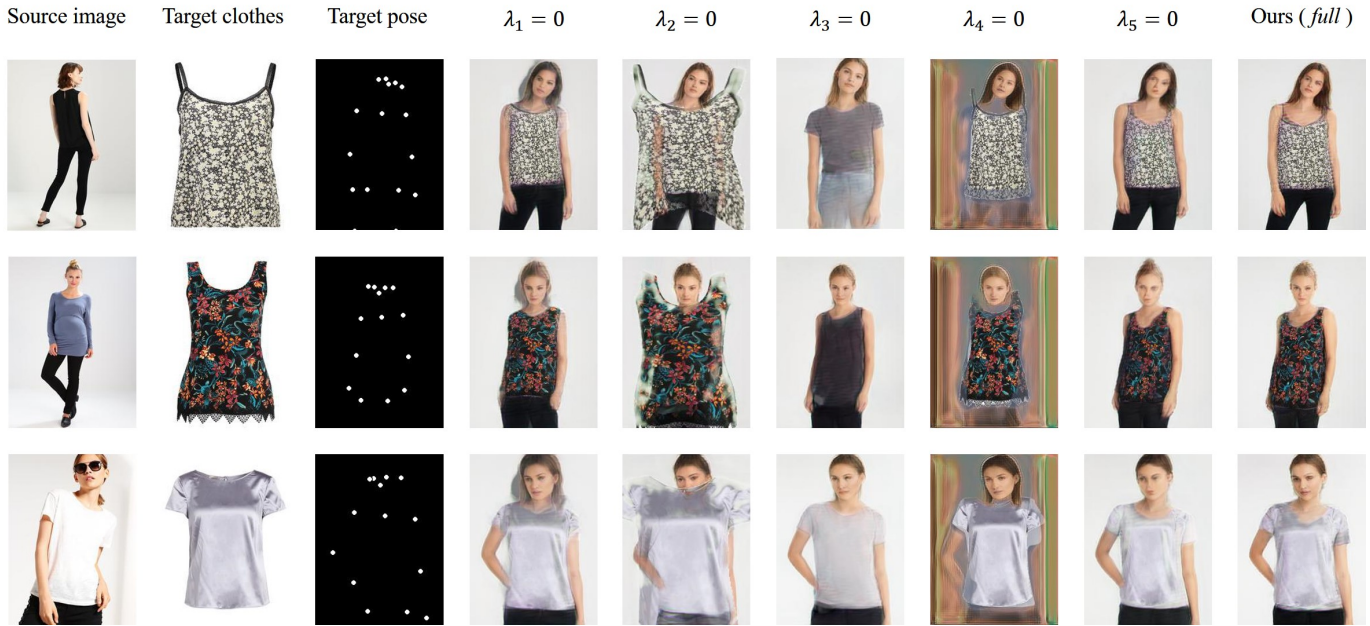


Fig. 7. Qualitative visual comparison of the full model with the variants obtained by setting each of the five hyper-parameters to zero.



Fig. 8. Examples of try-on results based on noisy images in the test set. For real-world applications, bags, sunglasses and Yuga mat are not desirable in the generated results. In this work, we view these objects as noise for the virtual try-on, and our method is still robust for such obstacles. The model has not seen the source inputs, which are all from the test set.

the clothes regions in the generated images is deformed, which shows that the conductible cycle consistency loss could alleviate the mismatching between the desired clothes and the target person image. In Fig. 6, we show the ablation study on the effect of conductible cycle consistency loss L_{cond} . Additionally, we observe artifacts in the non-clothing regions of the generated results after replacing the predicted target semantic

map with the predicted target body shape. This result indicates that without the guidance of the predicted semantic map, our method cannot accurately distinguish between regions of the human body. Moreover, we note that the facial regions in the generated results look less realistic after removing the global and local adversarial loss and the face identity loss, which suggests that introducing the global and local adversarial loss and the face identity loss can encourage the model to generate realistic and natural face regions. Also, we observe that removing the perceptual loss causes the model to generate blurred results with artifacts, suggesting that introducing the perceptual loss can synthesize sharper and clearer images.

We present the quantitative ablation study results of seven variants in TABLE IV. We observe that the full model obtains higher SSIM scores and Mask-SSIM scores than six different ablation methods except with the ground-truth semantic map. We also note that without the perceptual loss, the scores of IS/Mask-IS are higher than the whole model. It is due to the perceptual loss with deeper supervision (leveraging the activation of deeper layers), which focuses on the semantic patterns. Therefore, the full model with the perceptual loss will improve the SSIM matching quality to the ground-truth in terms of multiple scales, but fail to hold better global matching IS. We think this alternative is still open to the readers whether to use the perceptual loss or not and depends on the application which emphasizes the pair matching performance or the global comparison with the whole dataset. The qualitative visual results with/without the perceptual loss are also provided in Fig. 5. More importantly, the ablation studies also show that the conductible cycle consistency loss could match the shape of the deformed desired clothes with the target person image and maintain characteristics of the desired clothes in the generated try-on image. We present the qualitative visual results with/without the cycle consistency constraint in Fig. 5

and Fig. 6. The ablation studies also point out that using real semantic maps at test time yields higher metrics scores than predicted semantic maps, suggesting that the semantic maps obtained by the separate semantic prediction networks still have a gap with real semantic maps. However, we find that all metrics increase with an end-to-end training manner. In particular, the scores of IS/Mask-IS achieving superiority. This result indicates that adopting an end-to-end training manner can enhance the accuracy of predicted semantic maps and lead the model to generate realistic fitting images.

Impact of the introduced five hyper-parameters. To clarify the role of the five hyper-parameters introduced in the objective function (*i.e.*, Eq. 17), we first show the qualitative visual results for the full model with five variants in Fig. 7. We observe that when $\lambda_1 = 0$, our method can still generate plausible fitting images, but artifacts appear. The main reason is that when $\lambda_1 = 0$, the focal loss is invalid. Therefore, the quality of the semantic map generated by SPM only maintains the rough body outline but cannot precisely locate the position of each body component. In addition, when $\lambda_2 = 0$, our method cannot generate reasonable fitting images. The main reason is that when $\lambda_2 = 0$, both L_{recon}^p and L_{perc}^p are invalid, which leads to the inability of SPM to generate coarse results and predicted clothing masks, which are critical inputs for TSM and CWM, respectively. Meanwhile, when $\lambda_3 = 0$, we find that the details of the desired clothes are entirely lost in the generated images, which indicates that the conductible cycle consistency loss plays a vital role in the process of clothes deformation. Additionally, when $\lambda_4 = 0$, we notice that even though the details of the facial and clothing regions in the generated image are well maintained, the entire quality of the generated image is poor due to the lack of global constraints. We also observe that when $\lambda_5 = 0$, the face identity loss is invalid, resulting in less realistic facial regions in the generated results. Furthermore, we report the quantitative results of the effectiveness of five hyper-parameters in TABLE V. It can be found that the full model obtains the highest SSIM/Mask-SSIM scores as well as the highest Mask-IS scores for the clothing regions in the generated images. Combining the results of qualitative and quantitative experiments, we consider it necessary to introduce these five hyper-parameters. In addition, to determine the optimal value of the hyper-parameter λ_3 , we conduct additional experiments and present the quantitative results in TABLE VI. We first set the values of λ_3 to 0, 1, 5, 10, 20, 40, 80, and then the experimental results show that when $\lambda_3 = 20$, the highest scores are obtained for all indicators except for the Mask-IS scores for facial regions.

Impact of noisy images in the training set and the test set. We provide the qualitative visual results for virtual try-on based on noisy images (*i.e.*, source images with interference from attributes unrelated to the fitting task, such as backpacks, glasses, and Complicated backgrounds). As shown in Fig. 8, we observe that the proposed method is robust to such training noise and shows good scalability to the unseen test images during inference.

V. CONCLUSION

In this paper, we propose a novel multi-pose virtual try-on framework (SPG-VTON) based on semantic prediction guidance, which focuses on produce photo-realistic try-on results while fitting the desired clothes into an arbitrary pose of the same person. SPG-VTON consists of three sub-modules, including the semantic map prediction module, the clothes warping module, and the try-on synthesis module. On the one hand, we introduce a conductible cycle consistency loss that can alleviate the mismatching between the desired clothes and the target image. On the other hand, we also apply a face identity loss to make the face region of the final virtual try-on image looks natural and well-preserved identity of the source image. Extensive qualitative and quantitative experiments demonstrate that the proposed method outperforms previous state-of-the-art methods and has good scalability to the training data noise as well as the unseen test images during inference. In the future, we will continue to explore the application of the proposed method to the new fields, such as vehicle appearance design [50] and language-based cloth generation [51].

REFERENCES

- [1] P. Isola, J.-Y. Zhu, T. Zhou, and A. A. Efros, "Image-to-image translation with conditional adversarial networks," in *Proceedings of the IEEE conference on computer vision and pattern recognition*, 2017, pp. 1125–1134. 1, 2
- [2] J.-Y. Zhu, T. Park, P. Isola, and A. A. Efros, "Unpaired image-to-image translation using cycle-consistent adversarial networks," in *Proceedings of the IEEE international conference on computer vision*, 2017, pp. 2223–2232. 1, 2
- [3] T.-C. Wang, M.-Y. Liu, J.-Y. Zhu, A. Tao, J. Kautz, and B. Catanzaro, "High-resolution image synthesis and semantic manipulation with conditional gans," in *Proceedings of the IEEE conference on computer vision and pattern recognition*, 2018, pp. 8798–8807. 1, 2, 4, 8
- [4] T. Karras, S. Laine, and T. Aila, "A style-based generator architecture for generative adversarial networks," in *Proceedings of the IEEE Conference on Computer Vision and Pattern Recognition*, 2019, pp. 4401–4410. 1, 2
- [5] X. Han, Z. Wu, Z. Wu, R. Yu, and L. S. Davis, "Viton: An image-based virtual try-on network," in *Proceedings of the IEEE conference on computer vision and pattern recognition*, 2018, pp. 7543–7552. 1, 2, 3, 5, 6, 8, 9
- [6] B. Wang, H. Zheng, X. Liang, Y. Chen, L. Lin, and M. Yang, "Toward characteristic-preserving image-based virtual try-on network," in *Proceedings of the European Conference on Computer Vision (ECCV)*, 2018, pp. 589–604. 1, 2, 3, 5, 6, 8, 9
- [7] H. Dong, X. Liang, X. Shen, B. Wang, H. Lai, J. Zhu, Z. Hu, and J. Yin, "Towards multi-pose guided virtual try-on network," in *Proceedings of the IEEE International Conference on Computer Vision*, 2019, pp. 9026–9035. 1, 2, 3, 4, 5, 6, 7, 8, 9
- [8] R. Yu, X. Wang, and X. Xie, "Vtnfp: An image-based virtual try-on network with body and clothing feature preservation," in *Proceedings of the IEEE International Conference on Computer Vision*, 2019, pp. 10511–10520. 1, 3, 5, 6
- [9] X. Han, X. Hu, W. Huang, and M. R. Scott, "Clothflow: A flow-based model for clothed person generation," in *Proceedings of the IEEE International Conference on Computer Vision*, 2019, pp. 10471–10480. 1, 3, 5
- [10] T. Issenhuth, J. Mary, and C. Calauzènes, "End-to-end learning of geometric deformations of feature maps for virtual try-on," *arXiv preprint arXiv:1906.01347*, 2019. 1, 3
- [11] N. Zheng, X. Song, Z. Chen, L. Hu, D. Cao, and L. Nie, "Virtually trying on new clothing with arbitrary poses," in *Proceedings of the ACM International Conference on Multimedia*, 2019, pp. 266–274. 1, 3, 5, 6
- [12] Y. Han, Z. Ruihao, G. Xiaobao, L. Wei, Z. Wangmeng, and L. Ping, "Towards photo-realistic virtual try-on by adaptively generating-preserving image content," in *Proceedings of the IEEE Conference on Computer Vision and Pattern Recognition*, 2020. 1, 3, 5, 6

- [13] C.-L. Chou, C.-Y. Chen, C.-W. Hsieh, H.-H. Shuai, J. Liu, and W.-H. Cheng, "Template-free try-on image synthesis via semantic-guided optimization," *IEEE Transactions on Neural Networks and Learning Systems*, 2021. [1](#)
- [14] Y. Ge, Y. Song, R. Zhang, C. Ge, W. Liu, and P. Luo, "Parser-free virtual try-on via distilling appearance flows," in *Proceedings of the IEEE Conference on Computer Vision and Pattern Recognition*, 2021, pp. 8485–8493. [1](#)
- [15] X. Gao, Z. Liu, Z. Feng, C. Shen, K. Ou, H. Tang, and M. Song, "Shape controllable virtual try-on for underwear models," *arXiv preprint arXiv:2107.13156*, 2021. [1](#)
- [16] Z. Xie, X. Zhang, F. Zhao, H. Dong, M. C. Kampffmeyer, H. Yan, and X. Liang, "WAS-VTON: Warping Architecture Search for Virtual Try-on Network," in *Proceedings of the ACM International Conference on Multimedia*, 2021. [1](#)
- [17] Z. Liu, P. Luo, S. Qiu, X. Wang, and X. Tang, "Deepfashion: Powering robust clothes recognition and retrieval with rich annotations," in *Proceedings of the IEEE conference on computer vision and pattern recognition*, 2016, pp. 1096–1104. [2](#), [7](#)
- [18] I. Goodfellow, J. Pouget-Abadie, M. Mirza, B. Xu, D. Warde-Farley, S. Ozair, A. Courville, and Y. Bengio, "Generative adversarial nets," in *Advances in neural information processing systems*, 2014, pp. 2672–2680. [2](#), [4](#)
- [19] M. Mirza and S. Osindero, "Conditional generative adversarial nets," *arXiv preprint arXiv:1411.1784*, 2014. [2](#), [4](#)
- [20] Z. Zheng, L. Zheng, and Y. Yang, "Unlabeled samples generated by gan improve the person re-identification baseline in vitro," in *Proceedings of the IEEE international conference on computer vision*, 2017, pp. 3754–3762. [2](#)
- [21] H. Dong, X. Liang, Y. Zhang, X. Zhang, Z. Xie, B. Wu, Z. Zhang, X. Shen, and J. Yin, "Fashion editing with multi-scale attention normalization," *arXiv preprint arXiv:1906.00884*, 2019. [2](#)
- [22] M. Liu, Y. Ding, M. Xia, X. Liu, E. Ding, W. Zuo, and S. Wen, "Stgan: A unified selective transfer network for arbitrary image attribute editing," in *Proceedings of the IEEE Conference on Computer Vision and Pattern Recognition*, 2019, pp. 3673–3682. [2](#)
- [23] Z. Huang, Z. Zheng, C. Yan, H. Xie, Y. Sun, J. Wang, and J. Zhang, "Real-world automatic makeup via identity preservation makeup net," in *IJCAI*, 2020, pp. 652–658. [2](#)
- [24] L. Ma, X. Jia, Q. Sun, B. Schiele, T. Tuytelaars, and L. Van Gool, "Pose guided person image generation," in *Advances in Neural Information Processing Systems*, 2017, pp. 406–416. [2](#)
- [25] L. Ma, Q. Sun, S. Georgoulis, L. Van Gool, B. Schiele, and M. Fritz, "Disentangled person image generation," in *Proceedings of the IEEE Conference on Computer Vision and Pattern Recognition*, 2018, pp. 99–108. [2](#)
- [26] Z. Zheng, X. Yang, Z. Yu, L. Zheng, Y. Yang, and J. Kautz, "Joint discriminative and generative learning for person re-identification," in *Proceedings of the IEEE Conference on Computer Vision and Pattern Recognition*, 2019, pp. 2138–2147. [2](#), [8](#)
- [27] P. Esser, E. Sutter, and B. Ommer, "A variational u-net for conditional appearance and shape generation," in *Proceedings of the IEEE Conference on Computer Vision and Pattern Recognition*, 2018, pp. 8857–8866. [2](#)
- [28] D. P. Kingma and M. Welling, "Auto-encoding variational bayes," *arXiv preprint arXiv:1312.6114*, 2013. [2](#)
- [29] A. Grigorev, A. Sevastopolsky, A. Vakhitov, and V. Lempitsky, "Coordinate-based texture inpainting for pose-guided image generation," *arXiv preprint arXiv:1811.11459*, 2018. [3](#)
- [30] A. Siarohin, E. Sangineto, S. Lathuilière, and N. Sebe, "Deformable gans for pose-based human image generation," in *Proceedings of the IEEE Conference on Computer Vision and Pattern Recognition*, 2018, pp. 3408–3416. [3](#)
- [31] H. Dong, X. Liang, K. Gong, H. Lai, J. Zhu, and J. Yin, "Soft-gated warping-gan for pose-guided person image synthesis," in *Advances in neural information processing systems*, 2018, pp. 474–484. [3](#)
- [32] S. Song, W. Zhang, J. Liu, and T. Mei, "Unsupervised person image generation with semantic parsing transformation," in *Proceedings of the IEEE Conference on Computer Vision and Pattern Recognition*, 2019, pp. 2357–2366. [3](#)
- [33] F. L. Bookstein, "Principal warps: Thin-plate splines and the decomposition of deformations," *IEEE transactions on pattern analysis and machine intelligence*, vol. 11, no. 6, pp. 567–585, 1989. [3](#)
- [34] S. Belongie, J. Malik, and J. Puzicha, "Shape matching and object recognition using shape contexts," *IEEE transactions on pattern analysis and machine intelligence*, vol. 24, no. 4, pp. 509–522, 2002. [3](#)
- [35] I. Rocco, R. Arandjelovic, and J. Sivic, "Convolutional neural network architecture for geometric matching," in *Proceedings of the IEEE Conference on Computer Vision and Pattern Recognition*, 2017, pp. 6148–6157. [3](#), [4](#), [5](#)
- [36] W. Liu, Y. Wen, Z. Yu, M. Li, B. Raj, and L. Song, "Sphereface: Deep hypersphere embedding for face recognition," in *Proceedings of the IEEE conference on computer vision and pattern recognition*, 2017, pp. 212–220. [4](#), [7](#)
- [37] Z. Cao, T. Simon, S.-E. Wei, and Y. Sheikh, "Realtime multi-person 2d pose estimation using part affinity fields," in *Proceedings of the IEEE Conference on Computer Vision and Pattern Recognition*, 2017, pp. 7291–7299. [3](#)
- [38] K. Gong, X. Liang, D. Zhang, X. Shen, and L. Lin, "Look into person: Self-supervised structure-sensitive learning and a new benchmark for human parsing," in *Proceedings of the IEEE Conference on Computer Vision and Pattern Recognition*, 2017, pp. 932–940. [3](#), [4](#)
- [39] O. Ronneberger, P. Fischer, and T. Brox, "U-net: Convolutional networks for biomedical image segmentation," in *International Conference on Medical image computing and computer-assisted intervention*. Springer, 2015, pp. 234–241. [4](#)
- [40] Y. Yan, J. Xu, B. Ni, W. Zhang, and X. Yang, "Skeleton-aided articulated motion generation," in *Proceedings of the 25th ACM international conference on Multimedia*, 2017, pp. 199–207. [4](#)
- [41] J. Johnson, A. Alahi, and L. Fei-Fei, "Perceptual losses for real-time style transfer and super-resolution," in *European conference on computer vision*. Springer, 2016, pp. 694–711. [5](#), [6](#)
- [42] K. Simonyan and A. Zisserman, "Very deep convolutional networks for large-scale image recognition," in *International Conference on Learning Representations*, 2015. [5](#)
- [43] Z. Wang, A. C. Bovik, H. R. Sheikh, and E. P. Simoncelli, "Image quality assessment: from error visibility to structural similarity," *IEEE transactions on image processing*, vol. 13, no. 4, pp. 600–612, 2004. [7](#)
- [44] T. Salimans, I. Goodfellow, W. Zaremba, V. Cheung, A. Radford, and X. Chen, "Improved techniques for training gans," in *Advances in neural information processing systems*, 2016, pp. 2234–2242. [7](#)
- [45] D. Ulyanov, A. Vedaldi, and V. Lempitsky, "Instance normalization: The missing ingredient for fast stylization," *arXiv preprint arXiv:1607.08022*, 2016. [8](#)
- [46] B. Hu, Z. Zheng, P. Liu, W. Yang, and M. Ren, "Unsupervised eyeglasses removal in the wild," *IEEE Transactions on Cybernetics*, 2020, doi:[10.1109/TCYB.2020.2995496](#). [8](#)
- [47] X. Mao, Q. Li, H. Xie, R. Y. Lau, Z. Wang, and S. Paul Smolley, "Least squares generative adversarial networks," in *Proceedings of the IEEE international conference on computer vision*, 2017, pp. 2794–2802. [8](#)
- [48] L. Mescheder, A. Geiger, and S. Nowozin, "Which training methods for gans do actually converge?" *arXiv preprint arXiv:1801.04406*, 2018. [8](#)
- [49] D. P. Kingma and J. Ba, "Adam: A method for stochastic optimization," *arXiv preprint arXiv:1412.6980*, 2014. [8](#)
- [50] Z. Zheng, T. Ruan, Y. Wei, Y. Yang, and T. Mei, "Vehiclenet: Learning robust visual representation for vehicle re-identification," *IEEE Transactions on Multimedia (TMM)*, 2020, doi:[10.1109/TMM.2020.3014488](#). [12](#)
- [51] Z. Zheng, L. Zheng, M. Garrett, Y. Yang, M. Xu, and Y.-D. Shen, "Dual-path convolutional image-text embeddings with instance loss," *ACM Transactions on Multimedia Computing, Communications, and Applications (TOMM)*, vol. 16, no. 2, pp. 1–23, 2020, doi:[10.1145/3383184](#). [12](#)